

# Dark Matter and its Particle Candidates \* §

A. Bottino <sup>a</sup> and N. Fornengo <sup>b</sup>

<sup>a</sup> Dipartimento di Fisica Teorica, Università di Torino and INFN, Sezione di Torino, via P. Giuria 1, I-10125 Torino, Italy

<sup>b</sup> Instituto de Física Corpuscular – C.S.I.C.

Departamento de Física Teòrica, Universitat de València  
c./ Dr. Moliner 50, E-46100 Burjassot, València, Spain

E-mail: bottino@to.infn.it, fornengo@flamenco.ific.uv.es

## Abstract

In these lectures we first briefly review the main observational facts which imply that most part of matter in the Universe is not visible and some recent intriguing experimental data which would point to a significant contribution to  $\Omega$  due to a cosmological constant. We subsequently discuss some particle candidates for dark matter, with particular emphasis for the neutralino. We present the main properties of this particle, also in the light of the most recent experimental results in direct search for relic particles; furthermore, we discuss the perspectives for their indirect searches.

## 1. Dark Matter and Cosmology

The two pillars of standard cosmology are the Einstein equations

$$R_{\mu\nu} - \frac{1}{2}\mathcal{R}g_{\mu\nu} = 8\pi GT_{\mu\nu} + \Lambda g_{\mu\nu}, \quad (1)$$

(where  $R_{\mu\nu}$  is the curvature (Ricci) tensor,  $\mathcal{R}$  is its trace,  $T_{\mu\nu}$  is the stress-energy tensor,  $\Lambda$  the cosmological constant) and the Robertson-Walker metric

---

\*Lectures given at the Fifth School on Non-Accelerator Particle Astrophysics (Abdus Salam International Centre for Theoretical Physics, Trieste, June–July 1998), to appear in the School Proceedings (Eds. R.A. Carrigan, Jr., G. Giacomelli and N. Paver)

§Report no. DFTT 20/99, FTUV/99–24, IFIC/99–26

$$ds^2 = dt^2 - R^2(t) \left( \frac{dr^2}{1 - kr^2} + r^2 d\theta^2 + r^2 \sin^2 \theta d\phi^2 \right), \quad (2)$$

where  $R = R(t)$  is the cosmic scale factor and  $t, r, \theta, \phi$  are the comoving coordinates <sup>1,2,3,4,5</sup>.

We recall that Eq. (2) follows from the assumption that the distribution of matter and radiation in the Universe is isotropic and homogeneous. When the coordinates are appropriately rescaled, the values  $k = +1, 0, -1$  define the space curvature to be positive, zero and negative, respectively. Useful standard quantities for the description of the expanding Universe are the Hubble parameter (expansion rate of the Universe)  $H = \dot{R}/R$  and the deceleration parameter  $q = -\ddot{R} \cdot R/\dot{R}^2$ , whose values at present epoch are denoted as  $H_0$  and  $q_0$ .

By combining Eqs. (1) – (2), one obtains the Friedmann equation

$$\Omega_m + \Omega_\Lambda - k/(H^2 R^2) = 1, \quad (3)$$

where  $\Omega_m$  is the ratio of the average matter–energy density  $\rho$  to the critical density  $\rho_c = 3H^2/(8\pi G)$ ,  $\Omega_m = \rho/\rho_c$ , and  $\Omega_\Lambda = \Lambda/(3H^2)$ . The critical density is given by  $\rho_c = 1.9 \cdot 10^{-29} h^2 \text{ g cm}^{-3}$ , when the Hubble constant is parametrised as follows:  $h = H_0/(100 \text{ km s}^{-1} \text{ Mpc}^{-1})$ .

From Eqs. (1) – (2) it also follows that at present time, when the radiation contribution to  $\Omega$  can be set to zero, the value of the deceleration parameter is given by

$$q_0 = \frac{1}{2}\Omega_m - \Omega_\Lambda. \quad (4)$$

The features of the evolution of our Universe depend on the actual values to be assigned to the cosmological parameters previously defined. In what follows we briefly summarize some of the main observational data about these parameters.

## 2. Age of the Universe and Expansion Rate

The evaluation of the present age of the Universe,  $t_0$ , depends on the expansion rate and on the various components of  $\Omega$ ; therefore measurements of  $t_0$  and of the Hubble constant provide information on the size of  $\Omega_m$  and  $\Omega_\Lambda$  (see, for instance, Refs. <sup>2,6</sup>).

A recent determination of  $t_0$  provides the value:  $t_0 = 11.5 \pm 1.3 \text{ Gyr}$  <sup>7</sup>, with a 95% C.L. lower bound of 9.5 Gyr. Recent measurements of the Hubble constant by the Hubble Space Telescope Key project give the following range <sup>6,8</sup>:  $H_0 = 73 \pm 6(\text{stat}) \pm 8(\text{syst}) \text{ km s}^{-1} \text{ Mpc}^{-1}$ . In view of the still persisting sizeable spread in the  $h$  values, due to a host of independent measurements (for a review, see for instance <sup>6</sup>) in the following we will, conservatively, consider a rather wide range:  $0.5 \leq h \leq 0.9$ .

If, for sake of illustration, we take  $h \simeq 0.7$ , it is easy to show that  $t_0 \sim 11.5$  Gyr would require either  $\Omega_m \lesssim 0.3$  or  $\Omega_m \sim 0.5$ , according to whether or not we allow for a non-vanishing cosmological constant, such that  $\Omega_\Lambda = 1 - \Omega_m$ .

### 3. Observational Evidence for Dark Matter

The parameter  $\Omega_m$  may be derived from astronomical determinations of the average mass-to-light ratio  $M/L$  for various astrophysical objects (see, for instance, Ref. <sup>9</sup> for an updated review)

$$\Omega_m = \frac{M}{L} \frac{L}{\rho_c}, \quad (5)$$

where  $L$  is the luminosity density:  $L = 1.6 \cdot 10^8 h L_\odot \text{ Mpc}^{-3}$ . Using  $\rho_c = 2.8 \cdot 10^{11} h^2 M_\odot \text{ Mpc}^{-3}$ , one gets

$$\Omega_m = \frac{h^{-1}}{1500} \frac{M/L}{M_\odot/L_\odot}. \quad (6)$$

From the  $M/L$  ratio measured in stars,  $M/L \sim (3 - 9) M_\odot/L_\odot$  we obtain

$$0.002 h^{-1} \leq \Omega_{vis} \leq 0.006 h^{-1}. \quad (7)$$

#### 3.1. Rotational curves of spiral galaxies

Presence of dark matter in single galaxies is apparent from the flatness of the plot of the rotational velocities versus the galactocentric radius, well beyond the distribution of the visible matter. From these measurements one derives  $M/L \simeq 70 M_\odot/L_\odot (R_{halo}/100 \text{ kpc})$ . Then we obtain

$$\Omega_{halo} \sim 0.05 h R_{halo}/100 \text{ kpc}, \quad (8)$$

a result which, compared to the range (7) for  $\Omega_{vis}$ , is indicative of the presence of dark matter at the level of single galaxies.

#### 3.2. Clusters of galaxies

Existence of dark matter at the level of clusters of galaxies may be established by a number of methods: X-ray emission by hot gas in intra cluster plasma, measurements of velocity dispersion and strong gravitational lensing.

We report here some results derived from measurements of the X-ray emission <sup>10</sup>. For rich clusters of galaxies one finds  $M/L = (300 \pm 100) h M_\odot/L_\odot$ , which gives

$$\Omega_{cluster} \simeq 0.2 \pm 0.07. \quad (9)$$

The baryonic content  $\Omega_b$  is established to be:  $\sim 6 h^{-3/2}\%$  for gas and  $\gtrsim 4\%$  for stars; then

$$\frac{\Omega_b}{\Omega_{cluster}} \gtrsim 0.04 + 0.06h^{-3/2}. \quad (10)$$

On the other hand, the Big Bang nucleosynthesis provides the following estimate for  $\Omega_b$  <sup>9,11</sup>:

$$0.009 \lesssim \Omega_b h^2 \lesssim 0.02, \quad (11)$$

or, taking  $0.5 \leq h \leq 0.9$ ,  $0.01 \lesssim \Omega_b \lesssim 0.08$ . Combining this result with Eq.(10) we obtain

$$\Omega_{cluster} \lesssim 0.2 - 0.4. \quad (12)$$

### 3.3. Large-scale Velocity Flows

Distribution of matter over large scales may be inferred from the peculiar motion of the gravitationally-induced inflow. Let us consider the case of the Local Supercluster, centered near the Virgo cluster; we stay on the edge of this cluster, at a distance of  $R = 12 h^{-1}$  Mpc. The radial inward peculiar velocity averaged over the surface is given by <sup>12</sup>

$$\bar{v} = \frac{1}{3} H_0 R \delta_m \Omega^{0.6}. \quad (13)$$

where  $\Omega^{0.6}$  represents the factor due to expansion and  $\delta_m$  denotes the mass contrast, related to the contrast in galaxy counts ( $\delta_g$ ) by the relation  $\delta_m = \delta_g/b$ ,  $b$  being the bias factor. Using the observational values <sup>12</sup>:  $\bar{v} = 200 \pm 25$  km s<sup>-1</sup>,  $\delta_g = 2.3 \pm 0.7$ , and taking  $b \simeq 1$ , one obtains

$$\Omega_m \simeq 0.1_{-0.05}^{+0.1}. \quad (14)$$

### 3.4. A few first conclusions

From the previous evaluations for  $\Omega_{vis}$  and  $\Omega_m$ , and from the range for  $\Omega_b$  in Eq.(11) we derive the following important points:

- a large amount of matter in the Universe is not visible;
- some of this dark matter is baryonic;
- a significant amount of dark matter is non-baryonic.

As usual we divide particle dark matter into two categories: Hot Dark Matter (HDM) and Cold Dark Matter (CDM), according to whether the particles are relativistic or non-relativistic at their decoupling from the primeval plasma.

#### 4. Singling out different contributions to $\Omega$

We briefly report now some important observational results and analyses which provide further clues toward a determination of the various components to  $\Omega$ . The two main issues are: what, if any, is the size of  $\Omega_\Lambda$  and what is  $\Omega_m$  made of?

##### 4.1. Formation of cosmological structures

A standard method for testing different dark matter models is to compare the power spectrum of the density fluctuations  $P(k)$  with measurements of the Cosmic Microwave Background Radiation (CMBR) anisotropy and measurements of the two-point correlation function in galaxy surveys<sup>2,3,4,5</sup>. We recall that  $P(k)$  is the Fourier transform of the correlation function between the density contrasts at two different points in space. It is customary to assume for  $P(k)$  a power law, i.e.  $P(k) \propto k^n$ . The Harrison–Zel’dovich spectrum corresponds to  $n = 1$ . In the past, typically, the best performing cosmological models turned out to fall into the following categories:

- HCDM model characterized by  $\Omega = 1$  and the following composition:  $\Omega_b \simeq 0.1$ ,  $\Omega_\nu \simeq 0.2$ ,  $\Omega_{\text{CDM}} \simeq 0.7$ ;  $h \simeq 0.5$ , where  $\Omega_b$ ,  $\Omega_\nu$  and  $\Omega_{\text{CDM}}$  are the contribution due to baryons, neutrinos (as HDM particles) and to CDM particles, respectively.
- $\Lambda$ CDM model with  $\Omega = 1$  and  $\Omega_{\text{CDM}} \simeq 0.3$ ,  $\Omega_\Lambda \simeq 0.7$ ;  $h \simeq 0.7 - 0.8$ .
- TCDM model ( $\equiv$  tilted CDM model) with a power spectrum  $P(k) \propto k^{0.8}$  and  $\Omega = 1 = \Omega_{\text{CDM}} = 1$ ;  $h \simeq 0.5$ .

##### 4.2. Evidence for $\Omega_\Lambda \neq 0$ ?

Recent measurements of high-redshift supernovae of type Ia<sup>13,14,15</sup> point to an important contribution to  $\Omega$  due to  $\Lambda$ , with a relatively small contribution from  $\Omega_m$ . These data appear to be complementary to those derived from measurements of the CMBR<sup>16</sup>. The joint use of these two sets of data, together with some other observational data, singles out the following ranges:  $\Omega_m = 0.24 \pm 0.10$  and  $\Omega_\Lambda = 0.62 \pm 0.16$ <sup>17</sup>. These data and analyses are of the utmost interest for their potential implications, although a number of points need further clarification<sup>3</sup>.

One further hint for a rather low value of  $\Omega_m$  is provided by the time evolution of the number density of clusters. In Ref.<sup>18</sup> observational data on cluster abundance in the redshift range  $0 \lesssim z \lesssim 1$  is used to derive the estimate  $\Omega_m \simeq 0.2_{-0.1}^{+0.15}$ .

Though a cautionary attitude is in order here, it is important to remark that all these different ways of determining  $\Omega_m$  point to a relative small value for this quantity:  $\Omega_m \lesssim 0.3 - 0.4$ . This feature, if confirmed by further observational data, has profound implications for the phenomenology related to DM particle candidates, as will be illustrated in the following.

## 5. Particle candidates for dark matter

### 5.1. Baryons

As was already noticed in Sect. III, some contribution to DM is provided by baryons. This conclusion is drawn from the fact that the Big Bang nucleosynthesis provides the estimate  $0.009 \lesssim \Omega_b h^2 \lesssim 0.02$ , which, together with Eq. (7), implies  $\Omega_b > \Omega_{\text{vis}}$ .

Direct search for non-luminous baryonic dark matter, under the form of microlensing objects, has been undertaken since the seminal paper of Ref.<sup>19</sup>. Recent results are reviewed in <sup>9,20,21</sup>. The main features of the data may be summarized as follows. The EROS Collaboration <sup>22</sup> excludes that microlensing objects of masses in the range  $(5 \cdot 10^{-8} - 10^{-2}) M_\odot$  may make up more than 20% of the halo density, whereas the MACHO Collaboration <sup>23</sup> delimits a likelihood contour (at 95% C.L.) for masses  $\sim (10^{-1} - 1) M_\odot$  with a best-fit value for the halo fraction around 0.5. For further details see, for instance, Refs. <sup>9,20,21</sup>. For a critical view of the microlensing events, see Ref.<sup>24</sup>. An interesting scenario related to baryonic dark matter is the one depicted in Ref.<sup>25</sup>.

### 5.2. Non-baryonic DM candidates

Particle physics offers a large variety of particles, which would have decoupled from the primeval plasma at the time (freeze-out time), when the interaction rate became smaller than the cosmic expansion rate; these particles would then be floating around in our Universe as relics.

These fossil particles would or would not significantly contribute to the average cosmic density depending on their actual number density and mass. The most obvious example is provided by light fossil neutrinos, whose relic abundance may be easily evaluated (see, for instance Ref.<sup>2</sup>) and turns out to be

$$\Omega_\nu h^2 = \frac{\sum m_\nu}{93 \text{ eV}}, \quad (15)$$

where the sum is over the neutrino flavours (for each flavour, neutrino and antineutrino are counted together). Therefore the relevance of these fossil neutrinos for the Universe matter density depends on whether their mass is of order of a few eV or much smaller (provided neutrinos are massive at all).

Possible indications for non-vanishing neutrino masses are from: 1) solar neutrinos <sup>26,27</sup>, 2) atmospheric neutrinos <sup>28,29,30</sup>, and 3) the LSND experiment <sup>31</sup>. All these data refer to oscillation measurements, and then are not sensitive to individual neutrino masses, but only to differences in their squares. Typically, atmospheric neutrino experiments give  $\Delta m^2 \simeq (2 \div 6) \times 10^{-3} \text{eV}^2$ ; solar neutrino experiments can be explained either by a  $\Delta m^2 \simeq 10^{-5} \text{eV}^2$ , in case of matter-enhanced oscillations, or by a  $\Delta m^2 \simeq 10^{-10} \text{eV}^2$ , in case of vacuum oscillations; LSND data suggest  $0.2 \text{eV}^2 \lesssim \Delta m^2 \lesssim 2 \text{eV}^2$ . These results may be compatible with a sizeable value of relic abundance,  $\Omega_\nu \sim 0.2$ , such as preferred by some calculations of cosmological structures. However, if taken at their face values, they only imply  $\Omega_\nu \gtrsim 0.02 (0.5/h)^2$  <sup>32</sup>.

A different candidate is the axion, whose motivation in particle physics is related to the strong CP-problem in QCD <sup>33</sup>. A discussion of this candidate is beyond the scope of the present report; for a comprehensive review on its possible cosmological relevance and on the experimental efforts for detecting it as a relic particle, see for instance Ref. <sup>34</sup>.

Among the particle candidates for CDM the most favorite one is certainly the Lightest Supersymmetric Particle (LSP), under the condition that it is weakly interacting. This candidate is discussed in the following section.

## 6. Supersymmetric dark matter particles

In order to be a dark matter candidate a particle has to be weakly interacting and stable (or, at least, long lived on cosmological time-scales). A very interesting perspective for such a candidate is offered, in the framework of supersymmetric theories with R-parity conservation, by the lightest susy particle (provided this is indeed weakly interacting). Different candidates have been considered: the neutralino <sup>35</sup> or the sneutrino <sup>36</sup> in gravity mediated models, the gravitino <sup>37</sup> or messenger fields <sup>38</sup> in gauge mediated theories, the axino <sup>39</sup>, stable non-topological solitons (Q-balls) <sup>40</sup>, heavy non-thermal relics <sup>41</sup> or others.

Among the different candidates, the most promising one turns out to be the neutralino, since its relic abundance may be sizeable, at the level required to explain the CDM content of the Universe and, at the same time, its detection rates may be accessible to experimental searches of different kinds.

The phenomenology of neutralino dark matter has been studied extensively in the Minimal Supersymmetric extension of the Standard Model (MSSM) <sup>42</sup>. This model incorporates the same gauge group as the Standard Model and the supersymmetric extension of its particle content. The Higgs sector is slightly modified as compared to that of the Standard Model: the MSSM requires two Higgs doublets  $H_1$  and  $H_2$  in order to give mass both to down- and up-type quarks and to cancel anomalies. After electroweak symmetry breaking, the physical Higgs fields consist of two charged particles and three neutral ones: two scalar fields ( $h$  and  $H$ ) and one pseudoscalar ( $A$ ). The Higgs sector is specified at the tree level by two independent parameters: the

mass of one of the physical Higgs fields and the ratio of the two vacuum expectation values, usually defined as  $\tan\beta = \langle H_2 \rangle / \langle H_1 \rangle$ . The supersymmetric sector of the model introduces some other free parameters: the mass parameters  $M_1$ ,  $M_2$  and  $M_3$  for the supersymmetric partners of gauge fields (gauginos), the Higgs–mixing parameter  $\mu$  and, in general, all the masses of the scalar partners of the fermions (sfermions) and all the trilinear couplings which enter in the superpotential. In the MSSM it is generally assumed that the gaugino masses are related by expressions induced by grand–unification. Specifically, the two parameters which are relevant for neutralino phenomenology are linked by:  $M_1 = (5/3)\tan^2\theta_W M_2$ . The other usual assumptions are that all slepton mass parameters are taken as degenerate to a common value  $m_0$  and that all the trilinear couplings are vanishing except the ones of the third family which are set to a common value  $A$ . In summary, the free parameters of the model are six:  $M_2$ ,  $\mu$ ,  $\tan\beta$ ,  $m_A$ ,  $m_0$  and  $A$ .

The neutralinos are four mass–eigenstates defined as linear superpositions of the two neutral gauginos ( $\tilde{\gamma}$  and  $\tilde{Z}$ ) and the two neutral higgsinos ( $\tilde{H}_1$  and  $\tilde{H}_2$ )

$$\chi = a_1\tilde{\gamma} + a_2\tilde{Z} + a_3\tilde{H}_1 + a_4\tilde{H}_2 . \quad (16)$$

The lowest–mass eigenstate may play the role of the lightest supersymmetric particle in the MSSM, and may then constitute the dark matter candidate in this model. It will be called the neutralino tout–court and its mass denoted by  $m_\chi$ . To classify the nature of the neutralino it is useful to define a parameter  $P \equiv a_1^2 + a_2^2$ ; the neutralino is called a *gaugino*, when  $P > 0.9$ , a *higgsino* when  $P < 0.1$  and *mixed* when  $0.1 \leq P \leq 0.9$ .

The low–energy MSSM scheme is a phenomenological approach, whose basic idea is to impose as few model–dependent restrictions as possible. At a more fundamental level, it is natural to implement this phenomenological scheme within the supergravity (SUGRA) framework<sup>43</sup>. One attractive feature of the ensuing model is the connection between soft supersymmetry breaking and electroweak symmetry breaking, which would then be induced radiatively. Usually, the low–energy phenomenology of SUGRA theories constitutes a subset of the susy configurations which are considered in the MSSM. A typical characteristic of SUGRA models is in fact the presence of relatively strong correlations among the low–energy parameters, correlation which is absent in the MSSM. In this report we will discuss neutralino dark matter phenomenology in the less constrained MSSM model. Results for SUGRA schemes can be found in the papers listed in Ref.<sup>44</sup>

### 6.1. Neutralino relic abundance

Neutralinos decouple from the hot plasma in the early Universe when they are no longer relativistic. Their present abundance is calculated by solving the Boltzmann



equation for the evolution of the density of particle species<sup>2</sup> and can be written as:

$$\Omega_\chi h^2 = \mathcal{C} \frac{g_*^{1/2}(T_f)}{g_{*S}(T_f)} \frac{1}{\langle \sigma_{\text{ann}} v_r \rangle_{\text{int}}} \quad (17)$$

where

$$\mathcal{C} = \frac{s_0}{0.264 \rho_c M_P} = 8.7 \cdot 10^{-11} \text{ GeV}^{-2}. \quad (18)$$

In the previous Eqs.,  $g_*(T_f)$  and  $g_{*S}(T_f)$  denote the effective number of degrees of freedom for the energy density and for the entropy density, respectively, evaluated at the freeze-out temperature  $T_f$ ;  $\langle \sigma_{\text{ann}} v_r \rangle_{\text{int}}$  is the neutralino pair annihilation times the pair relative velocity, averaged over the neutralino thermal density distribution, integrated from the freeze-out temperature down to the present temperature;  $s_0$  denotes the present entropy density,  $\rho_c$  is the critical density and  $M_P$  is the Planck mass.

The critical quantity to be evaluated is the neutralino annihilation cross section, which, depending on the neutralino mass, can get contributions from the following final states : i) fermion-antifermion pair, ii) pair of neutral Higgs bosons, iii) pair of charged Higgs bosons, iv) one Higgs boson-one gauge boson, v) pair of gauge bosons. The diagrams contributing to the final state i) are Higgs-exchange Z-exchange diagrams in the s-channel, sfermion-exchange diagrams in the t-channel. For the other final states, the contributions come from Higgs and Z-diagrams in the s-channel, and either neutralinos or charginos exchange in the t-channel, depending on the electric charges of the final particles<sup>45,46</sup>. When the mass of the neutralino is close to the mass of another supersymmetric particle, the process of co-annihilation<sup>47,48</sup> can be present. In this case, the calculation of the annihilation cross section and of its thermal average has to take into account a large number competing interactions among the neutralino and its close-mass particles. In some special instances the relic abundance may be affected by co-annihilation effects by a sizeable amount<sup>48</sup>.

In Fig. 1 we show  $\Omega_\chi h^2$  as a function of the neutralino mass  $m_\chi$ <sup>45</sup>. We present here, as well as in the following, all the results in terms of scatter plots which are obtained by varying the supersymmetric parameters inside wide ranges. Naturally, the parameter space is constrained by experimental limits on Higgs bosons and supersymmetric particles searches (for recent updates, see<sup>49</sup>) and by measurements of rare processes, whose theoretical predictions are quite sensitive to supersymmetric contributions. At present, the most important is the decay  $b \rightarrow s + \gamma$ <sup>50,51</sup>.

The scatter plot of Fig. 1 is obtained by varying the supersymmetric parameters in the following ranges:  $20 \text{ GeV} \leq M_2 \leq 500 \text{ GeV}$ ,  $20 \text{ GeV} \leq |\mu| \leq 500 \text{ GeV}$ ,  $80 \text{ GeV} \leq m_A \leq 1000 \text{ GeV}$ ,  $100 \text{ GeV} \leq m_0 \leq 1000 \text{ GeV}$ ,  $-3 \leq A \leq +3$ ,  $1 \leq \tan \beta \leq 50$ .

The figure shows only those configurations which provide a value for the relic abundance lower than a cosmological upper bound which has been conservatively set as  $\Omega_\chi h^2 \leq 0.7$ . The susy configurations which entail larger values of  $\Omega_\chi h^2$  are

excluded by the lower limit on the age of the Universe <sup>7</sup>. This constraint is rather restrictive on the susy parameter space.

## 6.2. Detection of relic neutralinos

Relic neutralinos would act as CDM during the process of galaxy formation. It is therefore conceivable that they may constitute all or part of the dark matter halo. These neutralinos would be clustered in the Galaxy and hence possess a matter density distribution and a velocity distribution which depend on the dynamics of the Galaxy formation and evolution<sup>52</sup>.

Many different models have been discussed in the literature for the *matter density distribution*  $\rho(\vec{r})$  (see for instance Refs. <sup>53,54,55</sup>). This field is in rapid expansion, due to the high resolution simulations now at hand to investigate the structure of single galaxies <sup>56</sup>. In particular, these studies are expected to pin down the nature of the cuspy behaviour which appears to occur near the galactic center. Another very interesting possibility which is currently being investigated is that the halo could present a clumpy distribution of dark matter together with or in alternative to a smooth distribution. The uncertainties in the shape profile, combined with experimental uncertainties and the possibility that some fraction of the dark halo is made of baryonic dark matter in the form of MACHOS, implies that the local value of the matter density  $\rho_l = \rho(\vec{r}_\odot)$  is somewhat uncertain. At present, its most conservative range of variability can be set as <sup>57</sup>:  $0.1 \text{ GeV cm}^{-3} \leq \rho_l \leq 0.7 \text{ GeV cm}^{-3}$ .

The quantity  $\rho_l$  refers to the total dark matter density of the galactic halo. the neutralino local density is, in general, a fraction of it, i.e.  $\rho_\chi = \xi \rho_l$ , with  $\xi \leq 1$ . No exact way to evaluate the quantity  $\xi$  is currently available. A usual procedure is to consider the galactic halo as composed entirely of neutralinos if, on the average in the Universe, neutralinos are abundant enough to explain all the CDM which is observed at least on the galactic scale. This happens when  $\Omega_\chi h^2$  is larger than a value  $(\Omega h^2)_{\min}$  derived from astrophysical observations. In this case it is possible to set  $\xi = 1$ . If, on the contrary,  $\Omega_\chi h^2 < (\Omega h^2)_{\min}$ , neutralinos are not able to explain all the CDM, even the one which is needed at the galactic scale, and therefore also locally in our Galaxy we expect them to give only a fractional contribution  $\xi$  to  $\rho_l$ . In this case, the simplest choice is to set:  $\xi = \Omega_\chi h^2 / (\Omega h^2)_{\min}$ . The quantity  $(\Omega h^2)_{\min}$  is estimated to lie in the range  $0.01 \lesssim (\Omega h^2)_{\min} \leq 0.2$ .

The *velocity distribution*  $f(\vec{v})$  of dark matter is usually assumed to be a Maxwellian distribution <sup>52</sup> (as seen from the galactic rest frame), with a velocity dispersion  $v_{\text{rms}}$  which is directly related to the asymptotic flat rotational velocity  $v_\infty$  as:  $v_{\text{rms}} = \sqrt{3/2} v_\infty$ . In our Galaxy, the rotational velocity appears to be already flat at the local position, and therefore we set  $v_\infty = v_\odot$ . The experimental determination of the local rotational velocity is:  $v_\odot = 230 \pm 50 \text{ Km s}^{-1}$  (90 % C.L.)<sup>58</sup>. The distribution is also truncated by an escape velocity  $v_{\text{esc}}$  which falls in the range:  $v_{\text{esc}} = 450 \div 650 \text{ Km s}^{-1}$  (90 % C.L.)<sup>59,60</sup>. Modifications to the standard Maxwell–Boltzmann form have been

examined<sup>52,61</sup>, but the problem of determining the correct form of the distribution of the velocities in the halo has no clear and simple solution at present, both theoretically and observationally. Also the possibility that the halo could possess a bulk rotation has been considered in the literature<sup>62</sup>.

Due to the possibility that neutralinos are present in the halo of our Galaxy, it is of great interest, both for astrophysics and particle physics, to search for techniques capable of detecting these dark halo particles. Several methods have been proposed and in the following we will briefly review the ones which, at present, appear to be more promising.

### 6.3. Direct detection of relic neutralinos

The most direct possibility to detect dark matter particles is to look for their scattering with the nuclei of a low-background detector<sup>63</sup>. The interaction of slow halo neutralinos of mass  $m_\chi \gtrsim 25$  GeV with a detector produces the recoil of a nucleus with energy  $E_R$  of the order of few to tens keV. The recoil energy can be measured by means of various experimental techniques with different nuclear species, like Ge, NaI, Xe, CaF<sub>2</sub>, TeO<sub>2</sub><sup>64</sup>. The relevant quantity to be calculated and compared with the experimental measurements is the differential detection rate

$$S_0(E_R) \equiv \frac{dR}{dE_R} = N_T \frac{\rho_\chi}{m_\chi} \int d\vec{v} f(\vec{v}) v \frac{d\sigma}{dE_R}(v, E_R) \quad (19)$$

where  $N_T$  is the number of the target nuclei per unit of mass,  $\rho_\chi$  is the local neutralino matter density,  $\vec{v}$  and  $f(\vec{v})$  denote the neutralino velocity and velocity distribution function in the Earth frame ( $v = |\vec{v}|$ ). The nuclear recoil energy is given by  $E_R = m_{\text{red}}^2 v^2 (1 - \cos\theta^*)/m_N$ , where  $\theta^*$  is the scattering angle in the neutralino–nucleus center-of-mass frame,  $m_N$  is the nuclear mass and  $m_{\text{red}}$  is the neutralino–nucleus reduced mass. Finally,  $d\sigma/dE_R$  is the neutralino–nucleus differential cross section, which has a coherent contribution due to Higgs- and squark-exchange, and a spin dependent one which originates from the exchange of the Z boson and squarks. The coherent cross section is usually largely dominant over the spin-dependent one.

Eq.(19) refers to the situation of a monoatomic detector, like the Ge detectors. For more general situations, like for instance the case of NaI, the generalization is straightforward. From those experimental data on the nuclear recoil spectrum which do not provide a signal-to-background discrimination, upper limits to the neutralino–nucleus cross section as a function of the neutralino mass may be set by employing Eq.(19)<sup>65</sup>. In the case of coherent interaction, Fig. 2 shows, as a solid line, the present most stringent upper limit<sup>66</sup> on the quantity  $\xi \sigma_{\text{scalar}}^{(\text{nucleon})}$  vs.  $m_\chi$ , where  $\sigma_{\text{scalar}}^{(\text{nucleon})}$  denotes the scalar elastic cross section of a neutralino off a nucleon. The astrophysical parameters are chosen as:  $\rho_l = 0.3$  GeV cm<sup>-3</sup>,  $v_0 = 220$  Km s<sup>-1</sup>,  $v_{\text{esc}} = 550$  Km s<sup>-1</sup> and  $(\Omega h^2)_{\text{min}} = 0.01$ .

In this plot, we also show a scatter plot of the same quantity calculated in the MSSM<sup>67,68</sup>. The susy configurations have been varied in the ranges quoted in Sect.

6.1. We stress that the cosmological bound  $\Omega_\chi h^2 \leq 0.7$  has been applied<sup>69</sup>.

In the case of direct detection, a typical signature consists in the annual modulation of the detection rate<sup>71</sup>. During the orbital motion of the Earth around the Sun, the change of direction of the relic particle velocities with respect to the detector induces a time dependence in the differential detection rate, i.e.  $S(E_R, t) = S_0(E_R) + S_m(E_R) \cos[\omega(t - t_0)]$ , where  $\omega = 2\pi/365$  days and  $t_0 = 153$  days (June 2<sup>nd</sup>).  $S_0(E_R)$  is the average (unmodulated) differential rate defined in Eq.(19) and  $S_m(E_R)$  is the modulation amplitude of the rate. The relative importance of  $S_m(E_R)$  with respect to  $S_0(E_R)$  for a given detector, depends both on the mass of the dark matter particle and on the value of the recoil energy where the effect is looked at. Typical values of  $S_m(E_R)/S_0(E_R)$  for a NaI detector range from a few percent up to  $\sim 15\%$ , for neutralino masses of the order of 20–80 GeV and recoil energies below 8–10 KeV.

The search for the annual modulation effect is currently undertaken by the DAMA/NaI Collaboration<sup>72</sup>. The analysis of their data over two years of data-taking provides the indication of a modulated signal<sup>73</sup>. This result can be shown as the closed contour in the  $\xi\sigma_{\text{scalar}}^{(\text{nucleon})}$  vs.  $m_\chi$  plane displayed in Fig. 2. The region inside the contour is compatible with a modulation signal at  $2\text{-}\sigma$  level. The contour takes into account also the uncertainties in astrophysical velocities, as discussed in<sup>74</sup>. Fig. 2 shows that there exist susy configurations which would be able to explain such an effect. In the papers of Refs.<sup>74,75</sup> it has been proved that some of these configurations are explorable at accelerators and/or by WIMP indirect experiments and that the relevant relic neutralinos might behave as major components of cold dark matter. For an analysis of these configurations in a SUGRA scheme, see also Ref.<sup>76</sup>.

#### 6.4. Indirect detection: neutrino fluxes from Earth and Sun

Other ways of detecting dark matter neutralinos rely on the possibility to detect the products of neutralino annihilations. One perspective is to observe a neutrino signal coming from celestial bodies, namely Earth and Sun, where the neutralinos may have been captured and accumulated during the lifetime of the macroscopic body. The sequence of the physical processes which could produce these signals are: i) capture of relic neutralinos by the macroscopic bodies; ii) subsequent accumulation of these particles in a region around the centre of these celestial objects; iii) pair annihilation of the accumulated neutralinos which would generate, by decay of the particles produced in the various annihilation final states, an output of high-energy neutrinos. Since the process of annihilation takes place inside a medium (i.e., the interior of the Earth or the Sun), the annihilation process is perturbed as compared to the annihilation in vacuum. This effect can be effectively taken into account<sup>77</sup> by neglecting the contributions of the light quarks directly produced in the annihilation process or in the hadronization of heavy quarks and gluons, because these light particles stop inside the medium (Sun or Earth) before their decay. For the case of the Sun, also the energy loss of the heavy hadrons in the solar medium and the energy loss of neutrino themselves have to be considered<sup>77</sup>.

The differential neutrino flux is then calculated as

$$\frac{dN_\nu}{dE_\nu} = \frac{\Gamma_A}{4\pi d^2} \sum_{F,f} B_{\chi f}^{(F)} \frac{dN_{f\nu}}{dE_\nu} \quad (20)$$

where  $\Gamma_A$  denotes the annihilation rate,  $d$  is the distance of the detector from the source (i.e. the center of the Earth or the Sun),  $F$  denotes the neutralino pair annihilation final states,  $B_{\chi f}^{(F)}$  denotes the branching ratios into heavy quarks,  $\tau$  lepton and gluons in the channel  $F$ . The spectra  $dN_{f\nu}/dE_\nu$  are the differential distributions of the neutrinos generated by the  $\tau$  and by hadronization of quarks and gluons and the subsequent semileptonic decays of the produced hadrons. A detailed calculation of these spectra is usually performed by means of a Montecarlo simulation<sup>78</sup>. The spectra due to heavier final states, i.e. Higgs bosons, gauge bosons and t quark, can be computed analytically by following their decay chain down to the production of a b quark, c quark or a tau lepton, where the result of the Montecarlo simulation can be applied<sup>78,79</sup>.

The neutrino flux may be detected in a neutrino telescope by measuring the muons which are produced by  $\nu_\mu$  and  $\bar{\nu}_\mu$  interactions in the rock around the detector and then traverse it upwardly. Therefore, the signal consists of a flux of up-going muons, which is computed as

$$\frac{dN_\mu}{dE_\mu} = N_A \int_{E_\mu^{\text{th}}}^\infty dE_\nu \int_0^\infty dX \int_{E_\mu}^{E_\nu} dE'_\mu P_{\text{surv}}(E_\mu, E'_\mu; X) \frac{d\sigma_\nu(E_\nu, E'_\mu)}{dE'_\mu} \frac{dN_\nu}{dE_\nu}, \quad (21)$$

where  $X$  is the muon range in the rock,  $d\sigma_\nu(E_\nu, E'_\mu)/dE'_\mu$  is the charged current cross-section for the production of a muon of energy  $E'_\mu$  from a neutrino of energy  $E_\nu$  and  $P_{\text{surv}}(E_\mu, E'_\mu; X)$  is the survival probability that a muon of initial energy  $E'_\mu$  will have a final energy  $E_\mu$  after propagating along a path-length  $X$  inside the rock which surrounds the detector. The function  $P_{\text{surv}}(E_\mu, E'_\mu; X)$  therefore takes into account the energy losses of muons in the rock. In Eq.(21),  $E_\mu^{\text{th}}$  is the detector threshold energy, which for current neutrino telescopes like MACRO and Baksan is of about 1-2 GeV, and this is quite suitable for neutralino indirect detection, especially for neutralinos lighter than about 100 GeV. Large-area neutrino telescopes with higher threshold energies (above a few tens of GeV) are more suitable for heavier relic particles.

Experimentally, one searches for a statistically significant excess of up-going muons above the muon flux originated from atmospheric neutrinos. The different angular behaviour of the signal with respect to the atmospheric neutrino background, which has a rather flat distribution as a function of the zenith angle, is the handle for the signal-to-background discrimination. Clearly, the flux from the Sun can be pointed at directly towards the direction of the Sun. In the case of the flux from the Earth, the process of accumulation of neutralinos induces a rather peaked distribution of the neutrino source around the Earth's center. Indeed, the angular distribution is

$$G(\theta) \simeq 4m_\chi \alpha \exp(-2m_\chi \alpha \sin^2 \theta) \quad (22)$$

where  $\theta$  is the zenith angle and  $\alpha = 1.76 \text{ GeV}^{-1}$ . This means that for neutralinos (which are heavier than  $\sim 25 \text{ GeV}$ ) the signal is produced inside a region whose angular extension is less than about 10 degrees.

The experimental searches at neutrino telescopes have found no muon excess so far and therefore upper limits on the muon flux have been set. The solid line in Fig. 3a is the current most stringent experimental upper limit from the MACRO Collaboration<sup>80,64</sup> for the neutrino flux from the center of the Earth. Fig. 3b refers to the flux from the Sun.

Again, superimposed to the experimental limits, we show in Fig. 3a (Earth) and Fig. 3b (Sun) the susy scatter plot for the up-going muon signal  $\Phi_{\mu}^{\text{Earth}}$  and  $\Phi_{\mu}^{\text{Sun}}$ . The susy configurations have been varied in the ranges quoted in Sect. 6.1. The astrophysical parameters are  $\rho_l = 0.3 \text{ GeV cm}^{-3}$ ,  $v_0 = 220 \text{ Km s}^{-1}$ ,  $v_{\text{esc}} = 550 \text{ Km s}^{-1}$  and the cosmological bound  $\Omega_{\chi} h^2 \leq 0.7$  has been applied.

### 6.5. Indirect detection: antimatter and gamma rays

The annihilation process of dark matter neutralinos may take place also directly in the galactic halo. In this case, many different signals other than neutrinos are possible. These signals, at variance with the signals previously discussed, which depend only on local galactic properties, depend directly on the matter distribution of neutralinos over the whole Galaxy. Moreover, the propagation inside the Galaxy of the particles which constitute the signal is perturbed by the Galaxy itself, like, for instance, interactions with the interstellar medium or, in the case of charged particles, diffusion in random magnetic fields.

One of the most interesting possibility is the production of antimatter from neutralino annihilation in the halo. The fluxes have been calculated for production of antiprotons, antideuteron and positrons.

*Antiprotons*<sup>81,82</sup> and *Antideuterons*<sup>83</sup> can be produced by the decay and hadronization of the final state particles of the annihilation process. The differential rate per unit volume and unit time for the production of  $\bar{p}$ 's from neutralino pair annihilation is defined as

$$q_{\bar{p}}^{\text{susy}}(T_{\bar{p}}) = \langle \sigma_{\text{ann}} v \rangle \left( \frac{\rho_{\chi}(\vec{r})}{m_{\chi}} \right)^2 \sum_{F,h} B_{\chi h}^{(F)} \frac{dN_{\bar{p}}^h}{dT_{\bar{p}}}, \quad (23)$$

where  $\langle \sigma_{\text{ann}} v \rangle$  denotes the average over the galactic velocity distribution function of neutralino pair annihilation cross section  $\sigma_{\text{ann}}$  multiplied by the relative velocity  $v$  of the annihilating particles,  $T_{\bar{p}}$  is the antiproton kinetic energy and  $B_{\chi h}^{(F)}$  is the branching ratio for the production of quarks or gluons  $h$  due to the decay of the particles produced by neutralino annihilation into the final state  $F$ . Finally,  $dN_{\bar{p}}^h/dT_{\bar{p}}$  is the differential energy distribution of the antiprotons generated by hadronization of quarks and gluons. Notice that the rate depends on the square of the mass distribution function of neutralinos in the galactic halo  $\rho_{\chi}(\vec{r})$ . The rate of production of  $\bar{D}$  is clearly analogous to Eq.(23).

After being produced, antimatter propagates inside the Galaxy and it experiences both diffusion in the galactic magnetic field and energy losses, due to ionization, scattering, collision and others. The propagation of antiprotons in the galactic medium is properly calculated in a diffusion model where the Galaxy is described as composed of two zones, one for the disk and the other for the halo. The diffusion equation which governs the behaviour of antiprotons is

$$\vec{\nabla} \cdot (K \vec{\nabla} \psi_{\bar{p}}) - 2h\delta(z) \Gamma_{\bar{p}} \psi_{\bar{p}} + 2h\delta(z) q_{\bar{p}}^{\text{susy}}(r) - 2h\delta(z) \frac{\partial}{\partial E} \{b(E)\psi_{\bar{p}}\} = 0 \quad , \quad (24)$$

where  $\psi_{\bar{p}}$  denotes the antiproton density,  $K$  is the diffusion coefficient,  $h$  is the height of the galactic disk and  $\Gamma_{\bar{p}}$  is the collision probability with the interstellar medium and  $b(E)$  describes energy losses. An analogous equation holds for the antideuterons.

Solution of the diffusion equations gives the antiproton (or antideuterons) flux at the heliosphere boundaries (interstellar flux) as

$$\Phi_{\bar{p}}(\odot, T_{\bar{p}}) = \langle \sigma_{\text{ann}} v \rangle \frac{v_{\bar{p}}}{4\pi} \left( \frac{\rho_l}{m_{\chi}} \right)^2 \psi_{\bar{p}}^{\text{eff}}(\odot, T_{\bar{p}}) \cdot \sum_{F,h} B_{\chi^h}^{(F)} \frac{dN_{\bar{p}}^h}{dT_{\bar{p}}}, \quad (25)$$

where  $\psi_{\bar{p}}^{\text{eff}}(\odot, T_{\bar{p}})$  is obtained by solving Eq.(24).

Antimatter subsequently enters the heliosphere where it propagates against the solar wind before arriving at the Earth. The effect induced by the solar wind (solar modulation) is quite important at low kinetic energies, and introduces a time dependence into the calculation, since it is correlated with the 11 year solar cycle.

Both antiprotons and antideuterons can be produced also by the interaction of primary cosmic rays on the interstellar medium. This secondary antimatter fluxes constitute a background for the susy signal. The background fluxes have a different energy behaviour as compared to the the ones of susy origin. In particular, the low energy tail of the energy spectrum is the most interesting place to look at, since the signals have a somewhat flat behaviour, while the secondary fluxes are depressed by kinematical reasons<sup>84</sup>. This effect is stronger for antideuterons than for antiprotons. Therefore, the antideuteron flux presents some advantages of discrimination over background with respect to the antiproton flux, even if its smallness makes the detection harder to be achieved.

Fig. 4 show the antiproton flux<sup>81</sup>  $\Phi_{\bar{p}}$  vs. the neutralino mass for the susy configurations introduced in Sect. 6.1. The flux is calculated for a  $\bar{p}$  kinetic energy  $T_{\bar{p}} = 0.24$  GeV, to conform to the first BESS energy bin, and for a solar modulation phase close to the BESS data-taking periods. The horizontal line is the present upper limit derived from the BESS 95 and BESS 97 data<sup>85</sup>. We notice that antiproton measurement are already able to exclude some susy configurations which would imply a too large  $\bar{p}$  flux at low kinetic energies.

Fig. 5 shows the antideuteron flux<sup>83</sup>  $\Phi_{\bar{D}}$  vs. the neutralino mass for the same susy models. The flux is calculated for a  $\bar{D}$  kinetic energy  $T_{\bar{D}} = 0.24$  GeV/nucleon,

at the maximum of solar activity. The horizontal line is the sensitivity level which could be achieved by the AMS detector during the flight on space station.

*Positrons*<sup>86</sup> are produced again from the decay chain of the neutralino annihilation products. It is also possible to produce directly a pair of monochromatic electron–positron pair. The branching ratio for this process is usually very small, but some susy models can present a production rate strong enough to be at the level of the detector sensitivity<sup>86</sup>. The calculation of the positron flux is analogous to the one for antiprotons or antideuterons, with the inclusion of additional energy loss mechanisms: inverse Compton scattering on starlight and cosmic microwave background, and synchrotron radiation emission in the galactic magnetic field. The IS positron flux is then affected by the solar wind before coming to the Earth where it can be detected. Fig. 6, taken from Ref.<sup>86</sup>, shows a scatter plot of the positron flux  $\Phi_{e^+}$  integrated in the energy range 8.9 – 14.8 GeV, to conform to one of the HEAT data bins. The susy parameters have been varied in the ranges:  $0 \text{ GeV} \leq |M_2| \leq 5000 \text{ GeV}$ ,  $0 \text{ GeV} \leq |\mu| \leq 5000 \text{ GeV}$ ,  $0 \text{ GeV} \leq m_A \leq 10000 \text{ GeV}$ ,  $100 \text{ GeV} \leq m_0 \leq 30000 \text{ GeV}$ ,  $-3 \leq A \leq +3$ ,  $1 \leq \tan \beta \leq 60$ . Only configuration with  $0.025 \leq \Omega_\chi h^2 \leq 1$  are shown on the plot. The horizontal dashed line denotes the value of the background positrons of secondary origin calculated in Ref.<sup>87</sup>. The horizontal band represents the HEAT 94 data<sup>88</sup>.

The last possibility we consider here is the production of *diffuse gamma rays* or a *gamma line* (see Refs.<sup>89,90,91,92,93,94</sup> and references quoted therein). Diffuse photons are produced mainly through the decay of neutral pions originated from the hadronization of the neutralino annihilation products. A monochromatic gamma line, instead, is produced through the loop–processes  $\chi\chi \rightarrow \gamma\gamma$  and  $\chi\chi \rightarrow Z\gamma$ . In this case, the gamma line would constitute a particularly nice signature, since it is practically background free.

In both cases, the fluxes are usually rather low and, in order to have fluxes at the level of the detector sensitivities, some matter over-density is needed, like for example a singular dark matter halo<sup>90,92</sup> or a clumpy matter distribution<sup>93</sup>. Fig. 7, taken from Ref.<sup>93</sup>, shows a scatter plot of the gamma ray flux  $\Phi_{cont,\gamma}$  integrated above  $E_\gamma = 1 \text{ GeV}$ . The susy parameters have been varied in the same ranges defined above for the positron flux. Only configurations with  $0.025 \leq \Omega_\chi h^2 \leq 0.5$  are shown on the plot. The horizontal line denotes the integrated gamma ray flux measured by EGRET<sup>95</sup>. Fig. 8 from Ref.<sup>92</sup> shows the perspectives of a number of Air Cherenkov Telescopes for the measurements of the expected  $\gamma$ –ray line.

## 7. Conclusions

As we have seen above, the question of dark matter in the Universe presents a large number of intriguing facets of relevance for cosmology, astrophysics and particle physics. It represents a field in a very fast expansion, because of an impressive development in experimental activities as well as in theoretical investigations. Let us mention just some of the most promising avenues: a) Further observations and



analyses of high- $z$  Supernovae, of the Cosmic Microwave Background Radiation, and of the time evolution of the number density of clusters are expected to provide more conclusive information on  $\Omega_m$  and  $\Omega_\Lambda$ . b) New numerical simulations of cosmological structures should give a unique information about the (hot/cold) composition of dark matter and about crucial details on the dark matter density profile in single galaxies. c) Further accumulation of data in WIMP direct detection are expected to play a fundamental role in the process of the identification of dark matter particle candidates. Present experimental results have already allowed the pinning down of a sector of the supersymmetric parameter space, part of which can be explored at accelerator and by WIMP indirect searches. It has been proved that the relevant relic neutralinos might behave as major components of cold dark matter. No doubt that the connection of particle physics with the dark matter problem in the Universe is one of the most exciting and far-reaching field in astroparticle physics.

### Acknowledgments

This work was supported by DGICYT under grant number PB95-1077 and by the TMR network grant ERBFMRXCT960090 of the European Union.

1. S. Weinberg, *Gravitation and Cosmology* (J. Wiley & Sons, 1972).
2. E.W. Kolb and M.S. Turner, *The Early Universe* (Addison-Wesley, 1988).
3. P. J. E. Peebles, *Principles of Physical Cosmology*, (Princeton University Press, 1993).
4. M. Roos, *Introduction to Cosmology* (J. Wiley & Sons, 1994).
5. E.W. Kolb, Proceedings of the Fourth School on *Non-accelerator Particle Astrophysics* (Editors E. Bellotti, R.A. Carrigan Jr., G. Giacomelli and N. Paver, World Scientific, 1996).
6. W.L. Freedman, talk given at CAPP 98, CERN, Geneva, June 1998, <http://wwwth.cern.ch/capp98/programme.html>.
7. B. Chaboyer, P. Demarque, P.J. Kernan and L.M. Krauss, *Ap.J.* 494 (1998) 96.
8. B.F. Madore et al., *Nature* 395 (1998) 47.
9. M. Spiro, E. Aubourg and Palanque-Delabrouille, *Nucl. Phys. B (Proc. Supplements)* 70 (1999) 14.
10. S.D.M. White, J.F. Navarro, A. Evrard and C.S. Frenk, *Nature* 366 (1993) 429; D. White and A. Fabian, *Mon. Not. Roy. Astron. Soc.* 272 (1995) 72; L. Lubin, R. Cen, N.A. Bahcall and J.P. Ostriker, *Ap.J.* 460 (1996) 10.
11. K. Olive, *Nucl. Phys. B (Proc. Supplements)* 70 (1999) 521.
12. P.J.E. Peebles, Proceedings of the Smithsonian debate *Is Cosmology Solved?*, (PASP, to appear), *astro-ph/9810497*.
13. S. Perlmutter, *Nature* 391 (1998) 51.

14. S. Perlmutter, talk given at CAPP 98, CERN, Geneva, June 1998, <http://wwwth.cern.ch/capp98/programme.html>.
15. A.G. Riess et al., *astro-ph/9805201* (to appear in Astron. J.).
16. For a recent review see, for instance, C.R. Lawrence, D. Scott and M. White, report UBC-COS-98-04, *astro-ph/9810446*, and references therein.
17. C.H. Lineweaver, *astro-ph/9805326* (to appear in Astroph. J. Lett.).
18. N.A. Bahcall and X. Fan, *astro-ph/9804082* (to appear in National Academy of Sciences Proc.).
19. B. Paczyński, Ap. J. 304 (1986) 1.
20. M. Spiro, review talk at the 19th Texas Symposium, Paris, December 1998.
21. C. Stubbs, talk given at the 19th Texas Symposium, Paris, December 1998.
22. R. Ansari et al. (EROS Collaboration), Astronomy and Astrophysics 314 (1996) 94.
23. C. Alcock et al. (MACHO Collaboration), Ap. J. 299 (1996) 84.
24. K. Freese, B. Fields and D. Graff, *astro-ph/9901178*.
25. F. De Paolis, G. Ingrosso, Ph. Jetzer and M. Roncadelli, *astro-ph/9901033*.
26. A. Yu. Smirnov, talk at Neutrino 98, Takayama, June 1998, *hep-ph/9809481*.
27. M.B. Smy, *hep-ph/9903034*.
28. Y. Fukuda et al. (Super-Kamiokande Collaboration), Phys. Rev. Lett. 81 (1998) 1562.
29. F. Ronga (MACRO Collaboration), talk at Neutrino 98, Takayama, June 1998, *hep-ph/9810008*.
30. A. Habig, *hep-ph/9903047*.
31. C. Athanassopoulos et al., Phys. Rev. C54 (1996) 2685; Phys. Rev. Lett. 81 (1998) 81.
32. J.R. Primack and M.A.K. Gross, Proceedings of the X<sup>th</sup> Rencontres de Blois, *The Birth of Galaxies*, June 1998, *astro-ph/9810204*.
33. R.D. Peccei and H.R. Quinn, Phys. Rev. D16 (1977) 1791.
34. G. Raffelt, talk at Neutrino 98, Takayama, 1998, *hep-ph/9806506*.
35. Because of the relevance of and interest in the subject of neutralino dark matter, a complete list of references would be too long to be fitted in this short review. We will therefore refer here to some of the more recent relevant papers, where references to older papers can be found. An extensive compilation of references previous to 1996 can also be found in G. Jungman, M. Kamionkowski and K. Griest, Phys. Rep. 267 (1996) 195.
36. T. Falk, K.A. Olive and M. Srednicki, Phys. Lett. B339 (1994) 248; L.J. Hall, T. Moroi and H. Murayama, Phys. Lett. B424 (1998) 305.
37. E.J. Chun, H.B. Kim and J.E. Kim, Phys. Rev. Lett. 72 (1994) 1956; A. Borgani, A. Masiero and M. Yamaguchi, Phys. Lett. B386 (1996) 189.
38. S. Dimopoulos, G.F. Giudice and A. Pomarol, Phys. Lett. B389 (1996) 37; T. Han and R. Hempfling, Phys. Lett. B415 (1997) 161.
39. S.A. Bonometto, F. Gabbiani and A. Masiero, Phys. Rev. D 49 (1994) 3918.

40. A. Kusenko and M. Shaposhnikov, Phys.Lett. B418 (1998) 46; A. Kusenko, V. Kuzmin, M. Shaposhnikov and P.G. Tinyakov, Phys. Rev. Lett. 80 (1998) 3185.
41. D.J.H. Chung, E.W. Kolb and A. Riotto, Phys. Rev. Lett. 81 (1998) 4048.
42. H.P. Nilles, Phys. Rep. 110 (1984) 1; H.E. Haber and G.L. Kane, Phys. Rep. 117 (1985) 75; R. Barbieri Riv. Nuovo Cim. 11 (1988) 1.
43. L. E. Ibañez and C. Lopez, Nucl. Phys. B233 (1984) 511; J. Ellis and F. Zwirner, Nucl. Phys. B338 (1990) 317; M. Drees and M. M. Nojiri, Nucl. Phys. B369 (1992) 54; R. Arnowitt and P. Nath, Lectures at VII J. A. Swieca Summer School, Campos do Jordao, Brazil, 1993, *hep-ph/9309277*; J. L. Lopez, D.V. Nanopoulos and A. Zichichi, Riv. Nuovo Cim. (1994) 1; W. de Boer, Prog. Part. Nucl. Phys. (1994) 201; G. L. Kane, C. Kolda, L. Roszkowski and J. D. Wells, Phys. Rev. D 49 (1994) 6173; R. Rattazzi and U. Sarid, Phys.Rev D 53 (1996) 1553; X. Wang, J. Lopez and D. Nanopoulos, Phys. Lett. B348 (1995) 105; V. Barger, M. S. Berger and P. Ohmann, Phys. Rev. D 49 (1994) 4908.
44. V. Berezhinsky, A. Bottino, J. Ellis, N. Fornengo, G. Mignola and S. Scopel, Astropart. Phys. 5 (1996) 1; Astropart. Phys. 5 (1996) 333; R. Arnowitt and P. Nath, Phys. Rev. D56 (1997) 2820.
45. A.Bottino, V.de Alfaro, N.Fornengo, G.Mignola and M. Pignone, Astropart. Phys. 2 (1994) 67.
46. R. Arnowitt and P. Nath, Phys. Lett B299 (1993); H. Baer and M. Bhrluk, Phys. Rev. D 53 (1996) 597.
47. K. Griest and D. Seckel, Phys. Rev. D 43 (1991) 3191; S. Mizuta and M. Yamaguchi, Phys. Lett. B 298 (1993) 120; M. Drees and M. Nojiri, Phys. Rev. D 47 (1993) 376; J. Ellis, T. Falk and K. A. Olive, Phys. Lett. B444 (1998) 367.
48. J. Edsjö and P. Gondolo, Phys. Rev. D 56 (1997) 1879.
49. V. Ruhlmann-Kleider (DELPHI Collaboration), presentation at the LEPC Conference, November 1998; R. Clare (L3 Collaboration), *ibid.*
50. S. Glenn (CLEO Collaboration), preprint CLEO CONF 98-17, 1998, International Conference on High Energy Physics, Vancouver, 1998, paper 1011; R. Barate et al. (ALEPH Collaboration), CERN preprint CERN-EP/98-044, 1998.
51. S. Bertolini, F. Borzumati, A. Masiero and G. Ridolfi, Nucl. Phys. B353 (1991) 591; R. Barbieri and G.F. Giudice, Phys. Lett. B309 (1993) 86; R. Garisto and J.N. Ng, Phys. Lett. B315 (1993) 372; F.M. Borzumati, M. Drees and M.M. Nojiri, Phys. Rev. D 51 (1995) 341; J. Wu, R. Arnowitt and P. Nath, Phys. Rev. D 51 (1995) 1371; V. Barger, M.S. Berger, P. Ohmann and R.J.N. Phillips, Phys. Rev. D 51 (1995) 2438; K. Chetyrkin, M. Misiak and M. Münz, Phys. Lett. B400 (1997) 206; M. Ciuchini, G. Degrassi, P. Gambino and G.F. Giudice, CERN preprint CERN-TH/97-279, 1997, *hep-ph/9710335*; A. Czarnecki and W.J. Marciano, Brookhaven National

- Laboratory preprint BNL–HET–98/11, 1998, *hep-ph/9804252*; M. Ciuchini, G. Degrassi, P. Gambino and G.F. Giudice, CERN preprint CERN–TH/98–177, 1998, *hep-ph/9806308*.
52. J. Binney and S. Tremaine, *Galactic Dynamics* (Princeton Univ. Press, 1987).
  53. J.F. Navarro, C.S. Frenk and S.D.M. White, *Ap. J.* 462 (1996) 563.
  54. J.F. Navarro, C.S. Frenk and S.D.M. White, *Ap. J.* 490 (1997) 493.
  55. A.V. Kravtsov, A.A. Klypin, J.S. Bullock and J.R. Primack, *Astrophys. J.* 502 (1998) 48.
  56. B. Moore, T. Quinn, F. Governato, J. Stadel and G. Lake, *astro-ph/9903164*.
  57. E. Gates, G. Gyuk and M.S. Turner, *Phys. Rev. Lett.* 74 (1995) 3724; *Phys. Rev. D* 53 (1996) 4238; E. Gates, G. Gyuk and M.S. Turner, *Astrophys. J. Lett.* 449 (1995) L123; E. Gates, G. Gyuk and M.S. Turner, *astro-ph/9704253*, *Proceedings of the 18th Texas Symposium on Relativistic Astrophysics*, edited by A. Olinto, J. Frieman and D. Schramm (World Scientific, to appear).
  58. C.S. Kochanek, *Ap. J.* 457 (1996) 228.
  59. P.J.T. Leonard and S. Tremaine, *Ap. J.* 353 (1990) 486.
  60. K.M. Cudworth, *Astron. J.* 99 (1990) 590.
  61. N.W. Evans, *Mont. Not. R. Astr. Soc.* 260 (1993) 191.
  62. F. Donato, N. Fornengo and S. Scopel, *Astropart. Phys.* 9 (1998) 247; M. Kamionkowski and A. Kinkhabwala, *Phys. Rev. D* 57 (1998) 3256.
  63. M.W. Goodman and E. Witten, *Phys. Rev. D* 31 (1985) 3059.
  64. For an extensive and recent review of the different experimental efforts involved in direct detection, as well as indirect detection, see the Proceedings of TAUP 97, *Nucl. Phys. B (Proc. Suppl.)* 70 (edited by A. Bottino, A. Di Credico, P. Monacelli), January 1999.
  65. A. Bottino, F. Donato, G. Mignola, S. Scopel, P. Belli and A. Incicchitti, *Phys. Lett. B* 402 (1997) 113.
  66. R. Bernabei et al., *Phys. Lett. B* 389 (1996) 757.
  67. A. Bottino, V. de Alfaro, N. Fornengo, G. Mignola, S. Scopel, C. Bacci et al., *Phys. Lett. B* 259 (1992) 330; A. Bottino, V. de Alfaro, N. Fornengo, G. Mignola and S. Scopel, *Astropart. Phys.* 2 (1994) 77;
  68. M. Drees and M.M. Nojiri, *Phys. Rev. D* 48 (1993) 3483; P. Gondolo and L. Bergström, *Nucl. Phys. (Proc. Suppl.)* 48 (1996) 53; R. Arnowitt and Pran Nath, *Phys. Lett. B* 437 (1998) 344; V. A. Bednyakov and H. V. Klapdor-Kleingrothaus, *Phys. Rev. D* 59 (1999) 023514; T. Falk, A. Ferstl and K. A. Olive, *Phys. Rev. D* 59 (1999) 055009.
  69. In Ref. <sup>70</sup> it has been suggested that there may exist a population of WIMPs which were set into bound Earth-crossing solar orbits by a peripheral scattering of galactic WIMPs on the surface of the Sun, with subsequent gravitational perturbations by planets. These WIMPs would have a dispersion velocity smaller (roughly, by a factor of 10) than the usual one of galactic WIMPs and would enhance direct detection rates at very low nuclear recoils (of order of KeV). Estimates of the expected effects are provided in Ref. <sup>70</sup>.

- Using these results it turns out that the upper limits on  $\xi\sigma_{\text{scalar}}^{\text{nucleon}}$  of Ref. <sup>66</sup> already set bounds on the model parameters which are somewhat more stringent than the ones indicated in Ref. <sup>70</sup> (see also J.I. Collar, Phys. Rev. D59 (1999) 063514 for a similar conclusion). For instance, for WIMPs of this population one would have  $m_\chi \gtrsim 200$  GeV, unless  $\rho_l \lesssim 0.2$  GeV cm<sup>-3</sup>.
70. T. Damour and L.M. Krauss, Phys. Rev. Lett. 81 (1998) 5726 and Phys. Rev. D 59 (1999) 063509.
  71. A.K. Drukier, K. Freese and D.N. Spergel, Phys. Rev. D 33 (1986) 3495; K. Freese, J. Frieman and A. Gould, Phys. Rev. D 37 (1988) 3388.
  72. R. Bernabei et al., University of Rome Report No. ROM2F/98/27 (submitted for publication).
  73. R. Bernabei et al., Phys. Lett. B424 (1998) 195; R. Bernabei et al., University of Rome Report No. ROM2F/98/34 and INFN Report No. INFN/AE-98/20 (to appear in Phys. Lett. B).
  74. P. Belli, R. Bernabei, A. Bottino, F. Donato, N. Fornengo, D. Prospero and S. Scopel, *hep-ph/9903501*.
  75. A. Bottino, F. Donato, N. Fornengo and S. Scopel, Phys. Lett. B 423 (1998) 109; A. Bottino, F. Donato, N. Fornengo and S. Scopel, *hep-ph/9710295*, Torino University Report No. DFTT 61/97 (unpublished); A. Bottino, F. Donato, N. Fornengo and S. Scopel, *hep-ph/9808456*, Torino University Report No. DFTT 41/98 (to appear in Phys. Rev. D); A. Bottino, F. Donato, N. Fornengo and S. Scopel, *hep-ph/9808459*, Torino University Report No. DFTT 48/98 (to appear in Phys. Rev. D); A. Bottino, F. Donato, N. Fornengo and S. Scopel, Astropart. Phys. 10 (1999) 203.
  76. R. Arnowitt and P. Nath, *hep-ph/9902237*.
  77. S. Ritz and D. Seckel, Nucl. Phys. B304 (1988) 877.
  78. A. Bottino, N. Fornengo, G. Mignola, L. Moscoso, Astropart. Phys. 3 (1995) 65; A. Bottino, V. de Alfaro, N. Fornengo, A. Morales, J. Puigedon and S. Scopel, Mod. Phys. Lett. A7 (1992) 733; A. Bottino, V. de Alfaro, N. Fornengo, G. Mignola and M. Pignone, Phys. Lett. B265 (1991) 57.
  79. L. Bergström, J. Edsjö and P. Gondolo, Phys. Rev. D 58 (1998) 103519; L. Bergström, J. Edsjö, M. Kamionkowski, Astropart. Phys. 7 (1997) 147; F. Halzen, *hep-ph/9506304*.
  80. The MACRO Collaboration, M. Ambrosio et al., *hep-ex/9812020*.
  81. A. Bottino, F. Donato, N. Fornengo and P. Salati, Phys. Rev. D 58 (1998) 123503; A. Bottino, C. Favero, N. Fornengo and G. Mignola, Astropart. Phys. 3 (1995) 77.
  82. L. Bergström, J. Edsjö and P. Ullio, *astro-ph/9902012*; J.D. Wells, A. Moiseev, J.F. Ormes, *hep-ph/9811325*; T. Mitsui, K. Maki and S. Orito, Phys. Lett. B389 (1996) 169; P. Chardonnet, G. Mignola, P. Salati and R. Taillet, Phys. Lett. B384 (1996) 161.
  83. F. Donato, N. Fornengo and P. Salati, Valencia University preprint FTUV/99-9 and IFIC/99-9.

84. More detailed evaluations of the secondary antiproton spectrum at low energies are still in progress; for some recent advancements in this field see L. Bergström, J. Edsjö and P. Ullio, *astro-ph/9902012* and J.W. Bieber, R.A. Burger, R. Engel, T.K. Gaisser, S. Roesler, T. Stanev, *astro-ph/9903163*.
85. S. Orito, International Conference on High Energy Physics, Vancouver, 1998.
86. E.A. Baltz, J. Edsjö, Phys. Rev. D59 (1999) 023511.
87. L.V. Moskalenko and A. Strong, Astrophys. J. 493 (1998) 694.
88. S.W. Barwick et al. (HEAT Collaboration), Astrophys. J. 498 (1998) 779.
89. L. Bergström and J. Kaplan, Astropart. Phys. 2 (1994) 261 J. Silk and A. Stebbins, Astrophys. J. 411 (1993) 439; M. Urban et al., Phys. Lett. B 293 (1992) 149; H.U. Bengtsson, P. Salati and J. Silk, Phys. Rev. D 40 (1989) 3828.
90. V. Berezhinsky, A. Bottino and G. Mignola, Phys. Lett. B325 (1994) 136.
91. V. Berezhinsky, A. Bottino and V. de Alfaro, Phys. Lett. B274 (1992) 122
92. L. Bergström, P. Ullio and J.H. Buckley, Astropart. Phys. 9 (1998) 137.
93. L. Bergström, J. Edsjö, P. Gondolo and P. Ullio, Phys. Rev. D59 (1999) 043506.
94. P. Ullio and L. Bergström, Phys. Rev. D 57 (1998) 1962; L. Bergström and P. Ullio, Nucl. Phys. B504 (1997) 27; Z. Bern, P. Gondolo and M. Perelstein, Phys. Lett. B 411 (1997) 86.
95. P. Sreekumar et al., Astrophys. J. 494 (1998) 523.

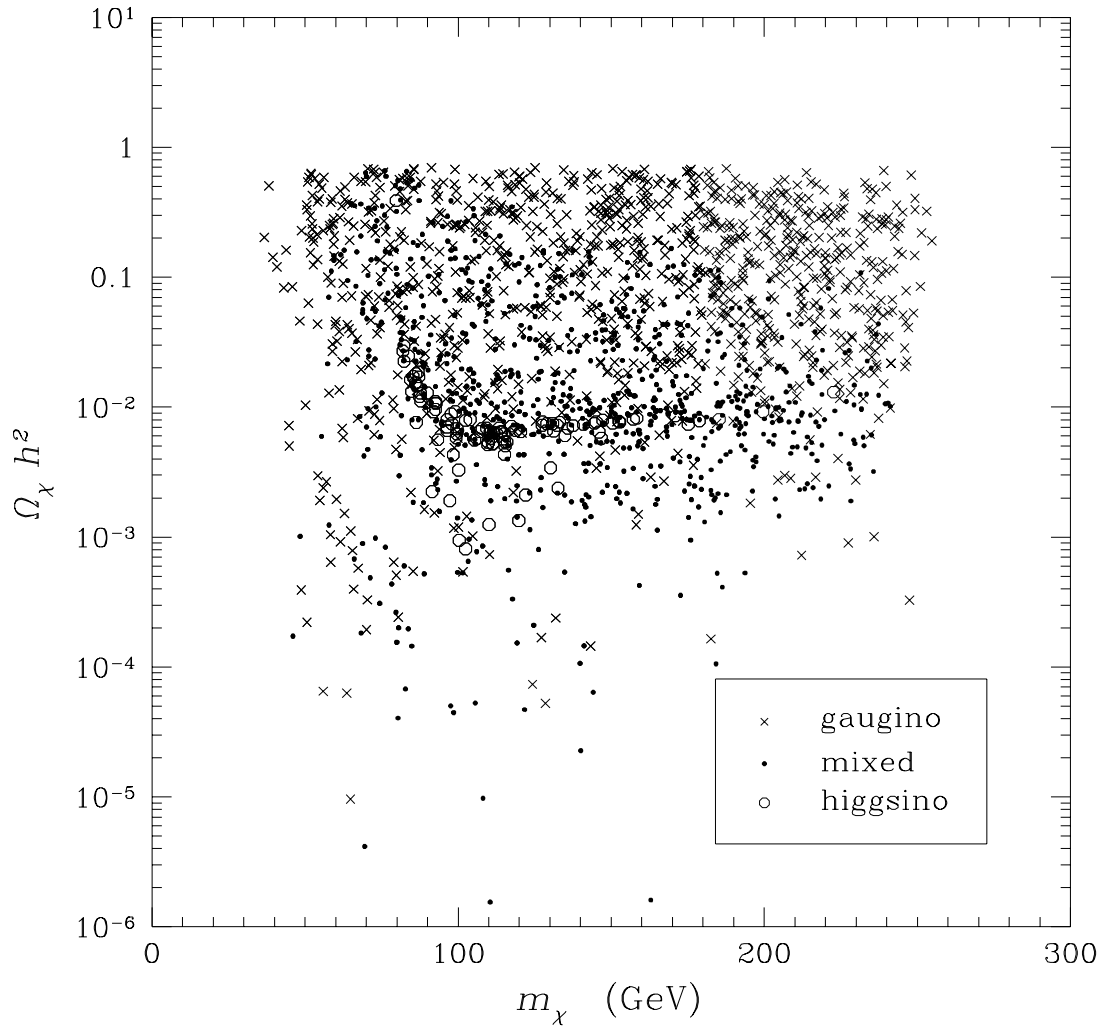


FIG. 1. Neutralino relic abundance  $\Omega_\chi h^2$  as a function of the neutralino mass  $m_\chi$ , evaluated in the MSSM. Only configurations which provide a relic abundance not in contrast with the age of the Universe (i.e.  $\Omega_\chi h^2 < 0.7$ ) are shown.

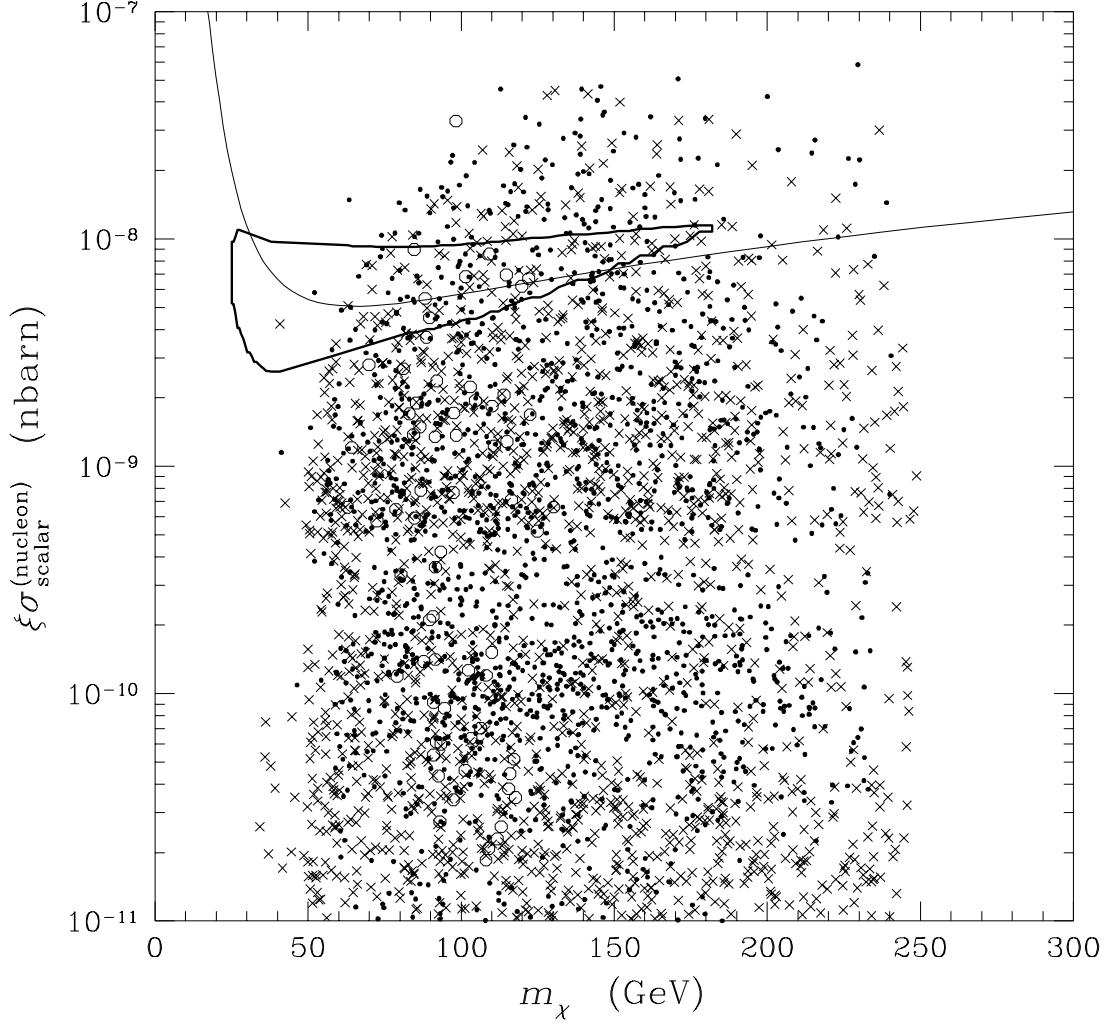


FIG. 2. Neutralino–nucleon cross section  $\sigma_{\text{scalar}}^{(\text{nucleon})}$  times the fractional amount of neutralino dark matter  $\xi$ , as a function of the neutralino mass  $m_\chi$ . The figure refers to the value  $\rho_l = 0.3 \text{ GeV cm}^{-3}$  for the total local dark matter density. The solid line is the present upper limit at 90% C.L.<sup>66</sup>. The closed contour delimits the region compatible with the annual modulation effect<sup>73,74</sup>. The scatter plot shows the quantity  $\xi \sigma_{\text{scalar}}^{(\text{nucleon})}$  evaluated in the MSSM. Different neutralino compositions are shown with different symbols: crosses for gauginos, open circles for higgsinos and dots for mixed neutralinos.



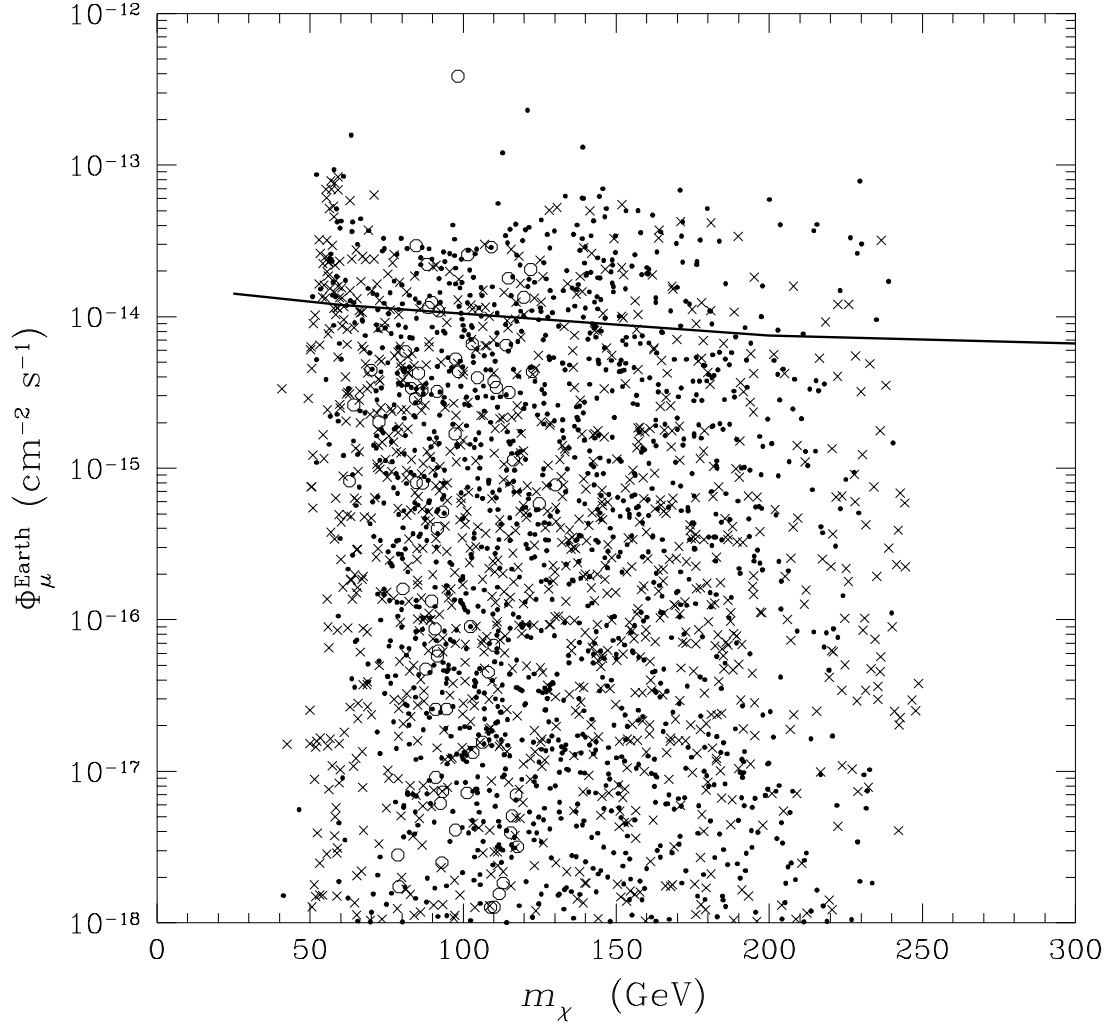


FIG. 3a. Flux of up-going muons  $\Phi_{\mu}^{\text{Earth}}$  from neutralino annihilation in the Earth, plotted as a function of  $m_{\chi}$ . The solid line denotes the present upper limit<sup>80</sup>. Different neutralino compositions are shown with different symbols: crosses for gauginos, open circles for higgsinos and dots for mixed neutralinos.

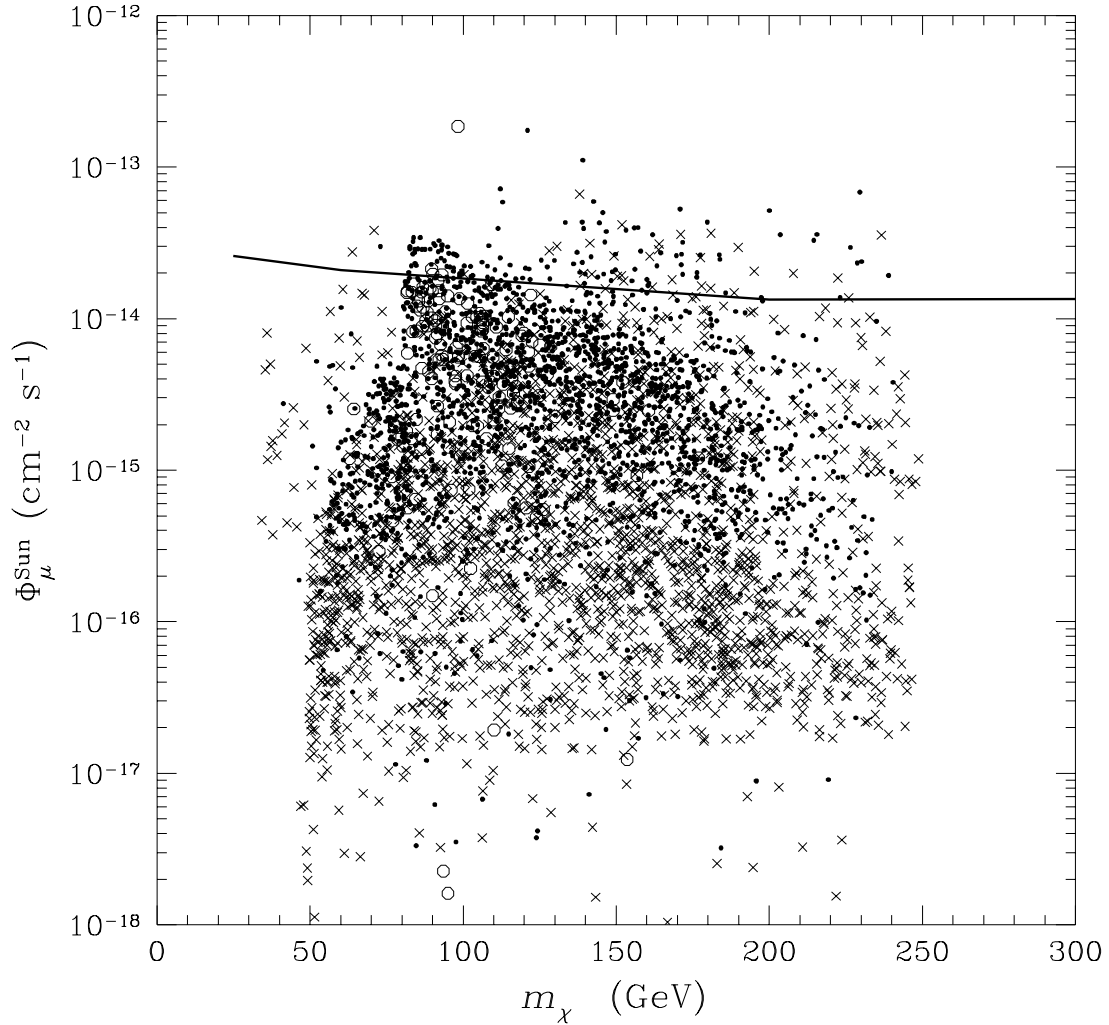


FIG. 3b. Flux of up-going muons  $\Phi_{\mu}^{\text{Sun}}$  from neutralino annihilation in the Sun, plotted as a function of  $m_{\chi}$ . The solid line denotes the present upper limit<sup>80</sup>. Different neutralino compositions are shown with different symbols: crosses for gauginos, open circles for higgsinos and dots for mixed neutralinos.

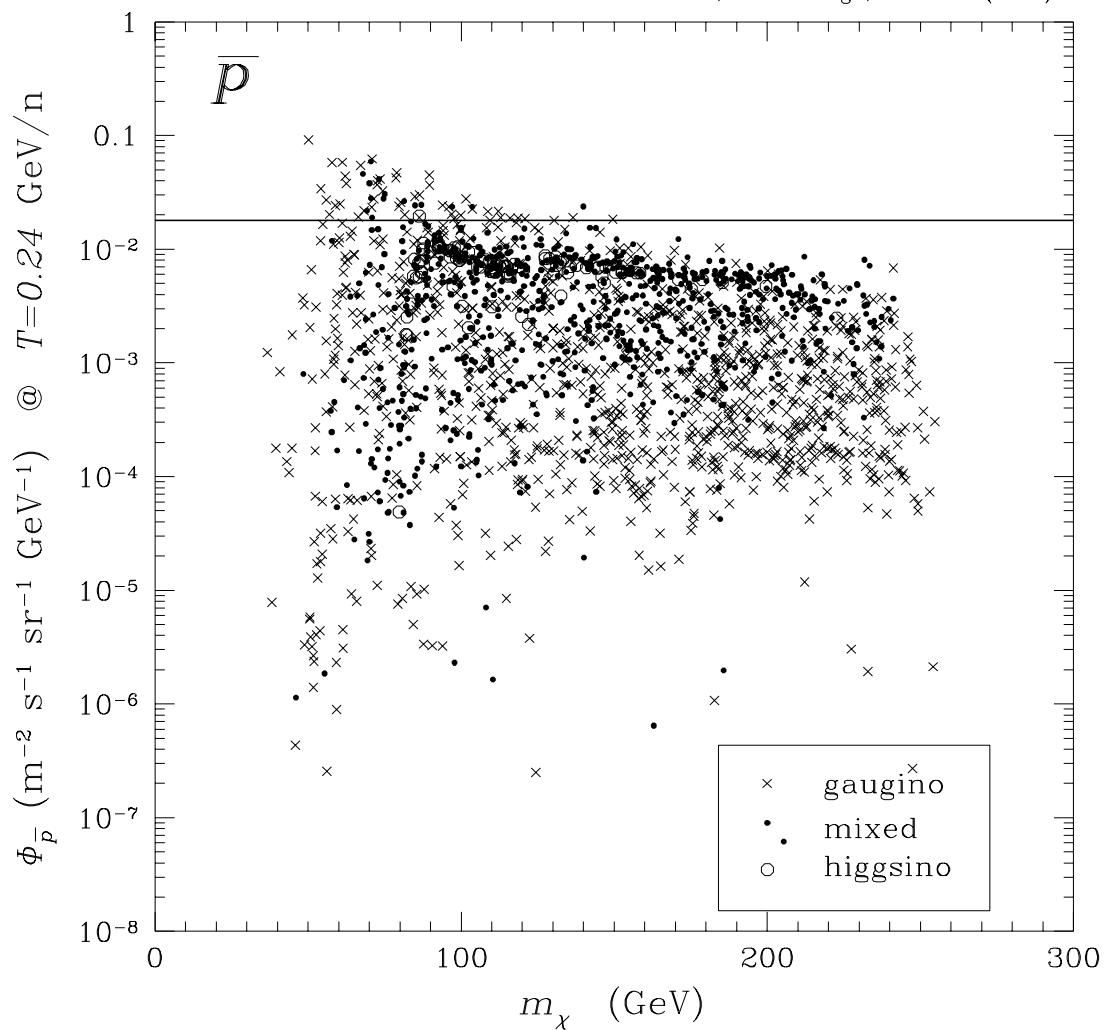


FIG. 4. Antiproton flux  $\Phi_{\bar{p}}$  as a function of  $m_\chi$  for a  $\bar{p}$  kinetic energy  $T_{\bar{p}} = 0.24$  GeV and for the solar minimum. The horizontal line is the present upper limit derived from the BESS 95 and BESS 97 data<sup>85</sup>.

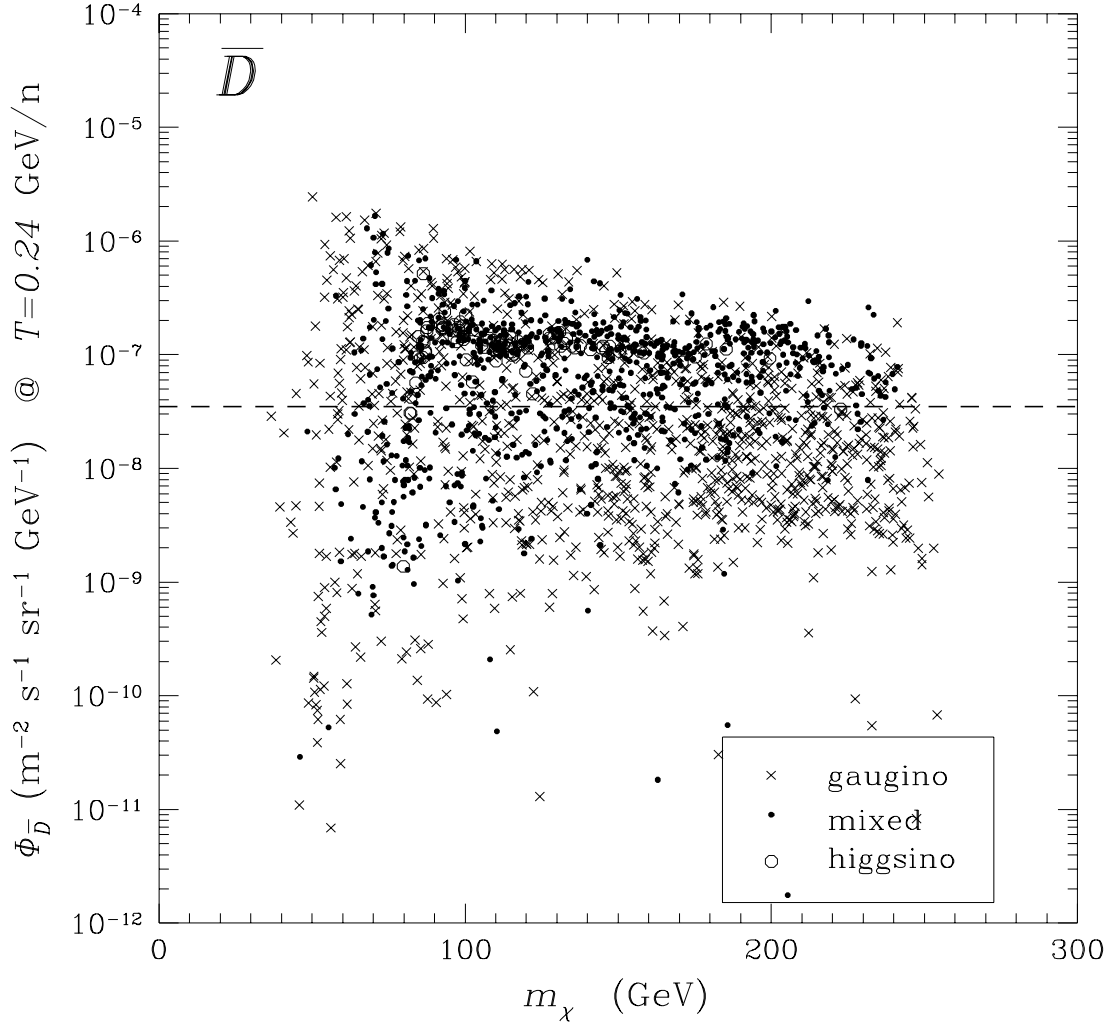


FIG. 5. Antideuteron flux  $\Phi_{\bar{D}}$  as a function of  $m_\chi$  for a  $\bar{D}$  kinetic energy  $T_{\bar{D}} = 0.24$  GeV and for the solar maximum. The horizontal line is the sensitivity that could be achieved by AMS during the flight on the space station <sup>83</sup>.

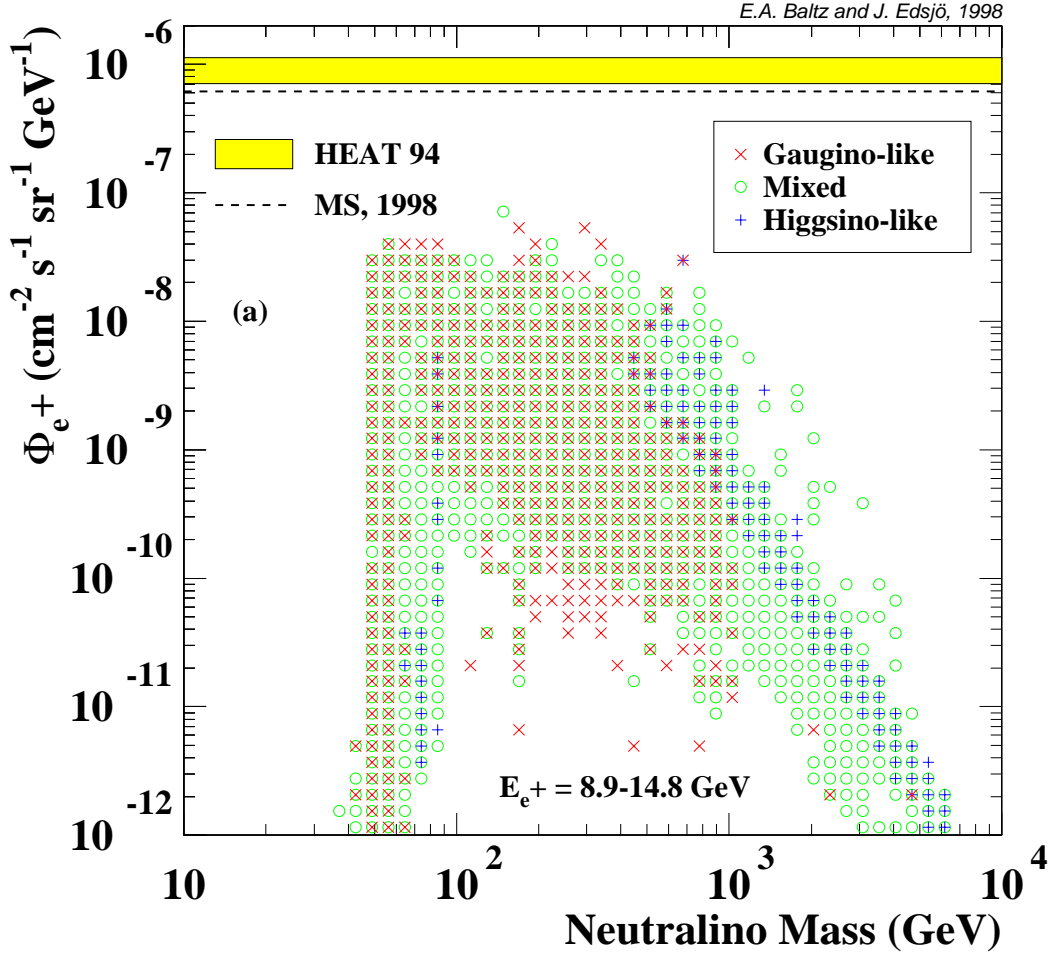


FIG. 6. Positron flux  $\Phi_{e+}$  integrated in the energy range 8.9 – 14.8 GeV vs.  $m_{\chi}$ , for configuration with  $0.025 \leq \Omega_{\chi} h^2 \leq 1$ . The horizontal dashed line denotes the value of the background positrons of secondary origin<sup>87</sup>. The horizontal band represents the HEAT 94 data.

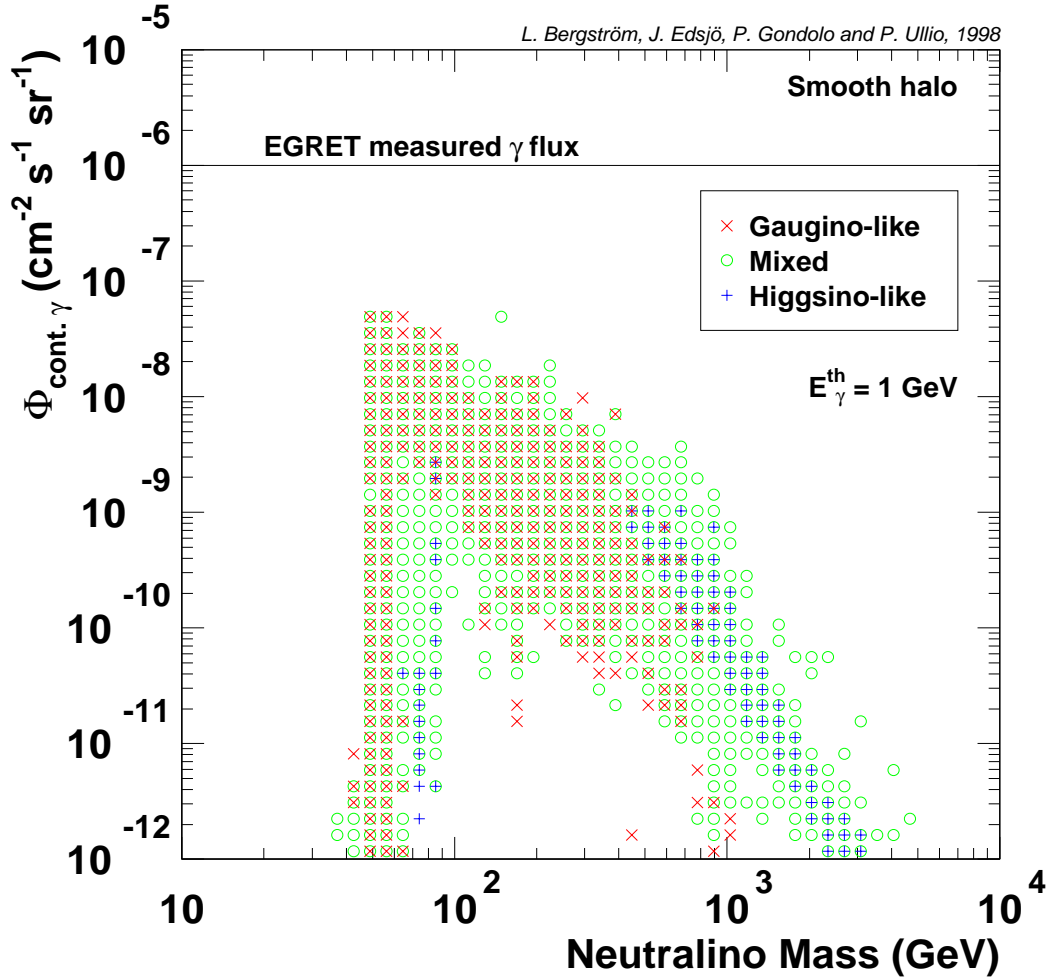


FIG. 7. Gamma ray flux  $\Phi_{cont,\gamma}$  integrated above  $E_{\gamma} = 1 \text{ GeV}$  vs.  $m_{\chi}$ , for configurations with  $0.025 \leq \Omega_{\chi} h^2 \leq 0.5$ . The horizontal line denotes the integrated gamma ray flux measured by EGRET<sup>95</sup>.

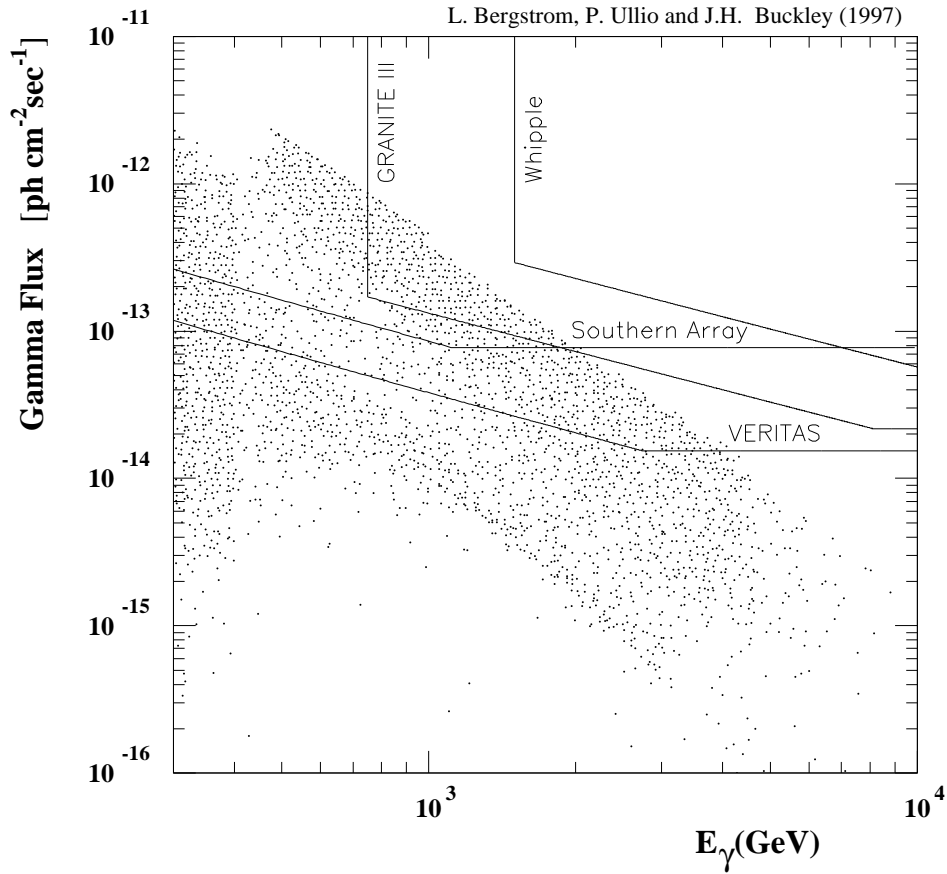


FIG. 8. Gamma ray flux inside a  $10^{-5}$  sr angular cone which contains the galactic center, for the density matter distribution of Ref.<sup>53</sup>. The flux refers to the contributions of the  $2\gamma$  and  $\gamma Z$  annihilation lines for heavy neutralinos. The solid lines denote the estimated sensitivities for different atmospheric Cherenkov detectors.